METEOROLOGICAL APPLICATIONS
Meteorol. Appl. (2018)
Published online in Wiley Online Library
(wileyonlinelibrary.com) DOI: 10.1002/met.1711

An overview of the micrometeorological field campaign at Santa Maria, Southern Brazil: the Pampa-2016 experiment

Gervásio Annes Degrazia,[a]* Umberto Rizza,[b] Michel Stefanello,[a] Silvana Maldaner,[c] Debora Regina Roberti,[a] Luis Gustavo Nogueira Martins,[a] Vagner Anabor,[a] Franciano Scremin Puhales,[a] Everson Dal Piva,[a] Otavio Costa Acevedo,[a] Hans Rogério Zimermann[a] and Cláudio Alberto Teichrieb[a]

[a] *Departamento de Física, Universidade Federal de Santa Maria, Brazil*
[b] *Institute of Atmospheric Sciences and Climate, National Research Council, Unit of Lecce, Italy*
[c] *Universidade Federal de Santa Maria – Campus de Cachoeira do Sul, Brazil*

ABSTRACT: The Pampa-2016 experimental campaign was performed in a typical Pampa lowland South American region. It consisted of both surface flux measurements (at 3 and 29 m) and a radiosonde launched every 3 h. The resulting meteorological observations allowed for the analysis of turbulent properties associated with both a stable and a convective boundary layer. The combined analysis of the surface data and vertical soundings has revealed some general characteristics of the atmospheric boundary layer for both the nocturnal stable conditions and the daytime convective environment. The continuous surface measurements showed that the nocturnal stable inversion, occurring in calm winds, is basically generated by the radiative cooling mechanism that is established after the late afternoon transition. The analysis of night-time surface data also showed that, under stable conditions in the case of vanishing wind speed, the friction velocity has unrealistic values that are very close to zero. This situation is undesirable for numerical models that generally use this quantity as a lower boundary condition. The analysis of night-time temperature profiles revealed two contrasting patterns in agreement with the classical classification of radiative night (a very stable boundary layer) and a turbulent night (a weakly stable boundary layer). In contrast, the analysis of the daytime temperature profiles provided an estimation of the convective time scale that is of the order of 10 min, in agreement with experimental values. A spectral analysis and the consequent estimation of the spectral peaks under unstable and stable conditions were in agreement with literature values.

KEY WORDS atmospheric boundary layer; field experiment; radiosounding profile

Received 15 September 2017; Revised 28 November 2017; Accepted 4 December 2017

1. Introduction

The atmospheric boundary layer (ABL) is the lowest part of the atmosphere in which a variety of complex motions, characterized by turbulence, may be present. In a diurnal cycle, the different manifestations of an ABL are generated by distinct forcing mechanisms that originate from mechanical and thermal effects which impart different depth scales and characteristic velocities to the ABL. For instance, a convective boundary layer (CBL) is defined by its depth z_i, which is usually taken as the height of the lowest inversion (Caughey, 1984), by a convective velocity scale w_* and by a friction velocity scale u_*. On the other hand, a stable boundary layer (SBL) is characterized by the depth of the nocturnal surface inversion (NSI), usually denoted by h_i (André and Mahrt, 1982; Garratt, 1992), and u_*.

During daytime, the positive turbulent heat flux establishes the structure of the CBL. Conversely, in a night-time stable ABL, the negative turbulent heat flux and clear-air radiative cooling, on average, control the development of the NSI layer.

Relevant periods occurring during the existence of an ABL concern transition situations, in which the turbulent heat flux switches sign and assumes positive and negative magnitudes. Over land and after sunrise the surface is warmed and heat is transferred upward by updrafts of warm air. Such a mechanism generates a deepening of the primitive CBL. In late afternoon, during sunset when the external forcing, such as the upward sensible heat flux and geostrophic forcing, varies rapidly, clear-air radiative cooling occurs and the turbulent heat flux decreases and becomes negative. In consequence, the convective turbulence decays with an accelerating rate (Rizza *et al.*, 2013a) and starts the formation of the NSI. Above the NSI, the convective energy-containing eddies start to lose their strength and mixing capacity, and the CBL begins to decay (Goulart *et al.*, 2003; Carvalho *et al.*, 2010; Rizza *et al.*, 2013aa, 2013b). This deep and near-adiabatic vertical region, which is the remnant of the daytime CBL, is known as the residual layer (Garratt, 1992). The use of precise information on this residual layer in numerical models is of fundamental importance when describing the evolution of the diurnal CBL (Blay-Carreras *et al.*, 2014).

Generally, experimental campaigns are important when used to describe the physical characteristics of the ABL. These observational studies usually employ automatic meteorological stations and radiosounding to measure the distinct characteristic parameters that allow for an understanding of the turbulent patterns occurring in a diurnal cycle of the ABL (Reuder *et al.*, 2012). In this context, the objective of the present study, named Pampa-2016, is to investigate the meteorological patterns and physical features of the ABL in a Pampa ecosystem region which

* Correspondence: G. A. Degrazia, Departamento de Física, Universidade Federal de Santa Maria, Santa Maria, RS, 97105-900, Brazil. E-mail: gervasiodegrazia@gmail.com

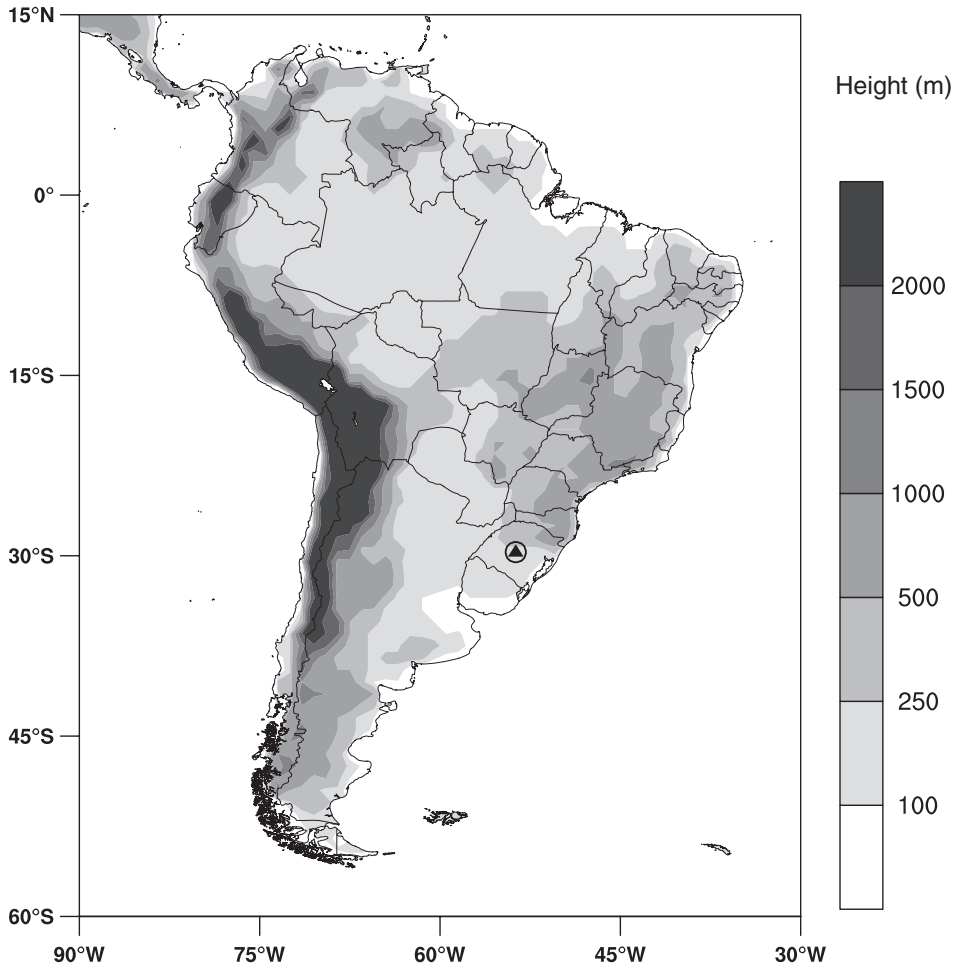

Figure 1. Experimental site in Santa Maria, RS, Brazil; the triangle shows the approximate location of the meteorological tower.

is a typical South American lowland. A micrometeorological tower equipped with a full suite of sensors was used. Furthermore, these surface data were complemented with radiosounding balloons that provided vertical profiles of the wind components and temperature. The analysis of the experimental data for this particular site reveals the turbulent characteristics of the daily cycle.

This region of South America has relatively few observational studies on meteorological and micrometeorological aspects. The evaluation and knowledge of these parameters, characterizing the ABL structure, can be applied in air pollution modelling, wind energy and numerical simulation at both a turbulence-resolving scale (large-eddy simulation) and mesoscale circulation (numerical weather prediction).

2. Method

The Pampa is a region located in southern Brazil, but which also covers large areas of Argentina and Uruguay (Figure 1). Its surface is mostly covered by natural grasslands, herbaceous plants and sparse trees. The experimental site was located in an area of 24 ha belonging to Biome Pampa in Santa Maria, RS, Brazil (29.7241 ° S, 53.759 ° W). There are no records or evidence that the field has suffered any kind of soil preparation for agricultural purposes, so it was assumed to have been a natural pasture for many centuries.

2.1. Instrumentation

At this experimental site, a flux tower of height 30 m instrumented with micrometeorological and soil sensors has collected data since 2013. These observed data are part of the SULFLUX (see http://www.ufsm.br/sulflux/) project, which was designed to help understand the interactions taking place between the atmosphere and the surface in south Brazil.

Sensor characteristics are described in Table 1. In the Pampa-2016 project, data on sonic anemometers situated at heights of 3 and 29 m, which were sampled at a frequency of 10 Hz, as well as integrated radiosounding meteorological data were used to evaluate the dynamic patterns of the ABL. The observations were made between 29 April and 1 May 2016. During the experiment, 17 radiosondes were launched, as described in Table 2.

The first radiosounding started at 1800 Local Time (LT) (UTC-3) on 29 April 2016; the last was taken at 2100 LT on 1 May 2016. The interval between soundings was 180 min.

2.2. Large-scale meteorological synoptic conditions

The experiment was carried out in a mid-latitude austral region. During the year, several synoptic transient systems reach southern Brazil, and in wintertime, the cold fronts arrive almost weekly. In the absence of synoptic transient systems, the weather is generally affected by a semi-permanent South Atlantic high pressure system. In addition, in summertime cold fronts are not

Table 1. Installed instruments at the experimental site.

Parameter	Manufacturer	Model	Height (m)
Wind speed	Campbell Scientific	CSAT3	29.0
Wind direction	Campbell Scientific	CSAT3	29.0
Air temperature	Campbell Scientific	CS215	30.0
Relative humidity	Campbell Scientific	CS215	30.0
Air temperature	Campbell Scientific	CS215	9.5
Relative humidity	Campbell Scientific	CS215	9.5
Wind speed	Campbell Scientific	IRGASON	3.0
Wind direction	Campbell Scientific	IRGASON	3.0
Air temperature	Campbell Scientific	CS215	3.0
Relative humidity	Campbell Scientific	CS215	3.0
Carbon dioxide concentration	Campbell Scientific	IRGASON	3.0
Water concentration	Campbell Scientific	IRGASON	3.0
Data logging	Campbell Scientific	CR1000	1.5

Table 2. Some basic features obtained from the radiosondes (Vaissala RS92).

Date in 2016	Start time (LT)	Maximum height (m)
29 April	1800	22 661
29 April	2100	24 892
30 April	0000	20 405
30 April	0300	24 059
30 April	0600	23 280
30 April	0900	23 062
30 April	1200	24 204
30 April	1800	23 451
30 April	2100	24 887
1 May	0000	25 527
1 May	0300	27 160
1 May	0600	27 310
1 May	0900	16 897
1 May	1200	25 050
1 May	1500	27 490
1 May	1800	6188
1 May	2100	14 220

as common (Grimm *et al.*, 2000). In particular, the PAMPA-2016 experiment occurred days after the first cold front of the year reached the experimental site. Furthermore, other weather systems acting in this region, such as mesoscale convective systems, are more frequent in spring and summer due the Chaco low pressure system (Anabor *et al.*, 2009).

During the experiment, transient anticyclones were acting over southern Brazil, and their centres moved from the southwest to the northeast between 29 April and 2 May, as seen in the reduced sea level pressure field (the continuous line) in Figure 2.

The general synoptic aspects (Figure 2) on 29 April show a small high pressure centre positioned close to the experimental area (triangle), and its weak pressure gradient resulted in calm conditions. The dashed lines in Figure 2 are the atmospheric layer thickness between the levels of 500 and 1000 hPa, given by the difference between the geopotential heights at these levels. As the thickness parameter is directly correlated with mean temperature in the atmospheric layers, there is no large-scale thermal advection because the thickness gradient is small. Thermal advection changes after the formation of a new anticyclone centred over Argentina during the next day, 30 April. The pressure gradient formed between the anticyclone centre and an extra tropical cyclone in the South Atlantic promotes cold advection to south Brazil, mainly over the coastal region. A cold tongue in the thickness field is formed, pushed by the southern large-scale flow. The cold advection over the south Brazilian coast persisted on 1 May, when the anticyclone centre was located over the experimental area, and again the pressure gradient and wind were weak. On 2 May, the anticyclone started its dissipation phase and the pressure gradient was reduced. This synoptic environment guaranteed cold weather, large-scale stability and calm winds during the experiment period.

3. Results

This section presents the analysis of the planetary boundary layer (PBL) structure in distinct stability conditions.

3.1. Surface parameters

Figure 3 presents the temporal evolution of the parameters that characterize the meteorological conditions occurring during the observational field campaign at a height of 3 m on the flux tower.

The magnitude of the wind speed was generally weak (Figure 3(a)), with 30 min averages below 3.5 m s^{-1} during daytime and magnitudes lower than 1.0 m s^{-1} during night-time. The temperature evolution (Figure 3(b)) exhibits a large amplitude, with values between 275 and 295 K. Such a large variation is a typical phenomenon for this period in southern Brazil. The solar irradiance (data not shown) reveals that 29 and 30 April were almost cloud free, while 1 May was completely cloud free. During night-time and the sunset transition, the wind speed was generally weak, causing a significant reduction in turbulence, which was responsible for the variations occurring in the low values of the turbulent kinetic energy (TKE) (Figure 3(c)). For daytime, the experimental turbulent fluxes, friction velocities, TKEs, flux Richardson numbers (Ri) and Obukhov lengths (L) were calculated with EddyPro software (Licor, 2015) using measured data at height 3 m obtained from 30 min time series. On the other hand, due to the low turbulence occurring at night-time, Ri and L were calculated using 5 min time series. Figure 4 shows the variation of the sensible heat flux (H) during the observational period. As a consequence of low TKEs, the sensible heat flux assumed negative and positive values (Hoover *et al.*, 2015).

Table 3 exhibits the means for the day- and night-time values for L and Ri. As a consequence of the low wind magnitudes, during the night L is small. The friction velocity (u_*) is defined in terms of the kinematic momentum flux. This flux can be expressed in terms of state variables:

$$u_* = \frac{kU(z)}{\ln\left(\frac{z}{z_0}\right) - \psi_m\left(\frac{z}{L}, \frac{z_0}{L}\right)} \tag{1}$$

where ψ_m is a stability correction function; U is the mean wind speed at a given height (3 m); and z_0 is the roughness length. There are several expressions for the stability correction function in the literature: the classic formulation of Businger (1971) (hereinafter 'B71') and a more recent from Beljaars and Holtslag (1991) (hereinafter 'BH91') have been chosen. These formulations analysed experimental data collected at Cabauw, the Netherlands, and informed a different formulation for stability function during stable conditions.

Figure 5 reports the comparison between the friction velocity calculated using B71 (dashed line) and BH91 (continuous line)

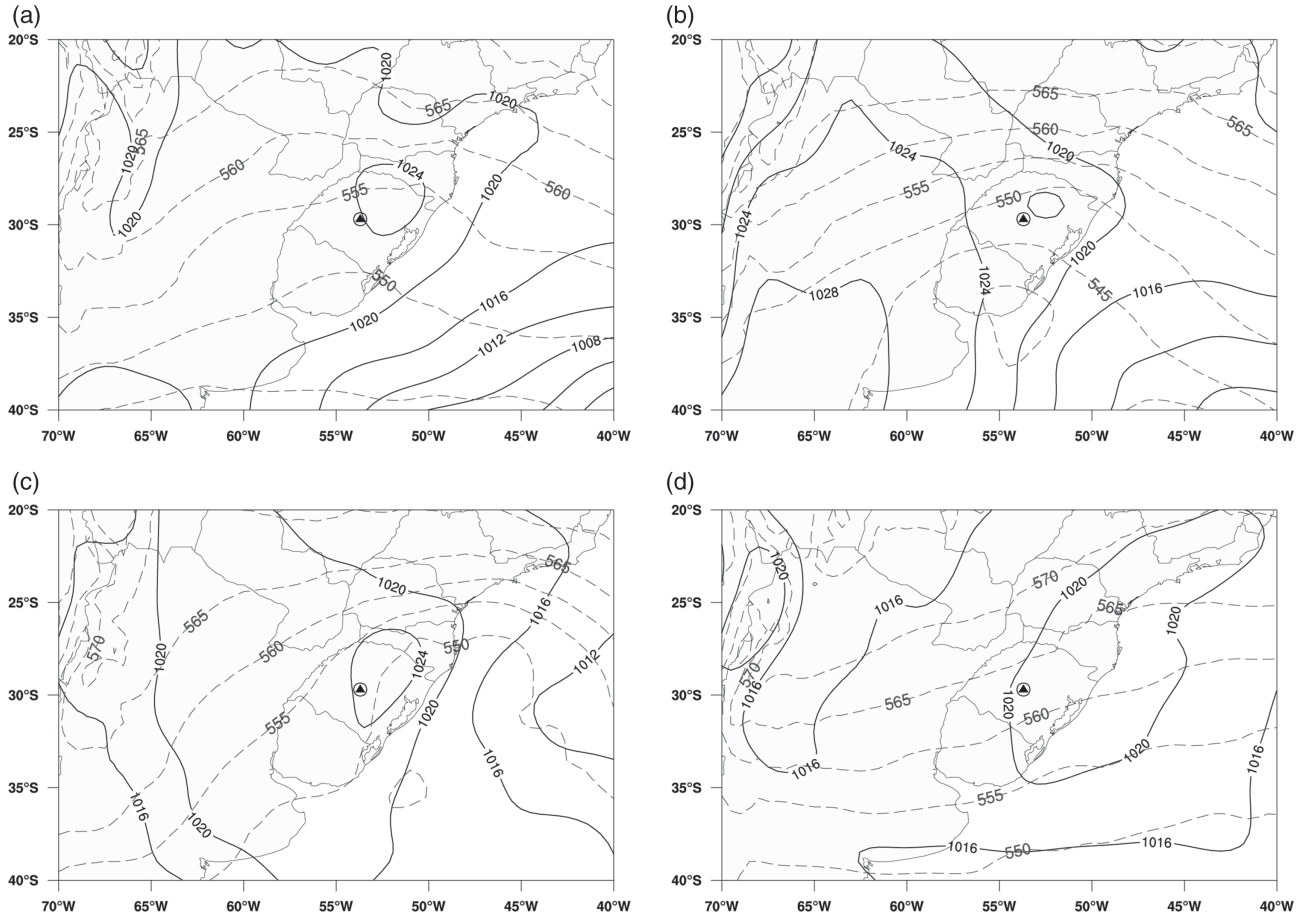

Figure 2. Synoptic conditions experienced during the experimental campaign: (a) 29 April at 2100 LT, (b) 30 April at 2100 LT, (c) 1 May at 2100 LT and (d) 2 May 2016 at 2100 LT. The black continuous line is the reduced sea level pressure (hPa); the grey dashed lines are the atmospheric layer thickness between 500 and 1000 hPa (in decametres). The triangle shows the location of the meteorological tower.

with the experimental data at 3 m (asterisks). Results are shown for each day of the experimental campaign, that is, (a, b) for April 29, (c, d) for April 30 and (e, f) for May 1. The B71 and BH91 functions in the left panels (a, c, e) are calculated using $z_0 = 0.05$ m, while the right panels (b, d, f) are calculated with the roughness parameter equal to 0.30 m. Note that during the daily hours of each experimental day, the best fit is obtained when using $z_0 = 0.30$ m. On the contrary, after sunset and before sunrise, the best fit is obtained using $z_0 = 0.05$ m. These results show the difficult in selecting an average roughness parameter for the whole experimental period. Note, too, that both B71 and BH91 give comparable results for the central daily hours, when the PBL is under unstable conditions, and as expected there are some slight differences for the stable hours probably caused by the intermittent nature of the stable PBL.

The overall statistical analysis computed with R-software (R Core Team, 2015) is reported in Table 4, from which it can be deduced that the BH91 formulation has a lower deviation (−9.90%) from the experimental mean. Note that under stable conditions (night-time) for wind speeds close to zero, that is, for the periods denoted P1–P3 in Table 5, the prediction obtained using Equation (1) gives values close to zero for both formulations. This singularity on friction velocity may lead to infinite values for similarity functions (B71). As a consequence, stability scaling parameters such as friction velocity become ill-defined and therefore the classical similarity theory (Vickers and Mahrt, 2006; Trini Castelli *et al.*, 2014), describing the turbulent transfer processes in the surface layer, should be revised under these conditions. Thus, it is a necessary new parameterization that prevents the surface stress and scalar fluxes from tending towards zero under low wind conditions (Andreas *et al.*, 2015).

3.2. Night-time temperature profiles

The surface data were complemented with radiosonde data that provided vertical profiles for wind components and temperature. The radiosondes were launched every 3 h, starting from 29 April at 1800 LT. The preliminary analysis concerns the potential temperature profile, which provides interesting information about the NSI and the ABL stable structure.

Figure 6 shows the potential temperature profile for distinct launch times in the SBL from 29 April 1800 LT to 30 April 0600 LT. The transition from the CBL to the SBL, which occurred close to 1800 LT, is also shown.

Two contrasting patterns were observed during the night of 29–30 April. In the first half of the period, from sunset to midnight, weak wind speeds, lower than 1.0 m s^{-1} (Figure 3(a)), were associated with reduced turbulent activity and an almost negligible downward sensible heat flux (Figure 4). As a consequence, the period was dominated by radiative processes, causing strongly curved potential temperature profiles during this first half of the night (1800/2100/0000 LT profiles of Figure 6), in agreement with the characterization proposed by André and Mahrt (1982). After midnight, on the other hand, wind speeds

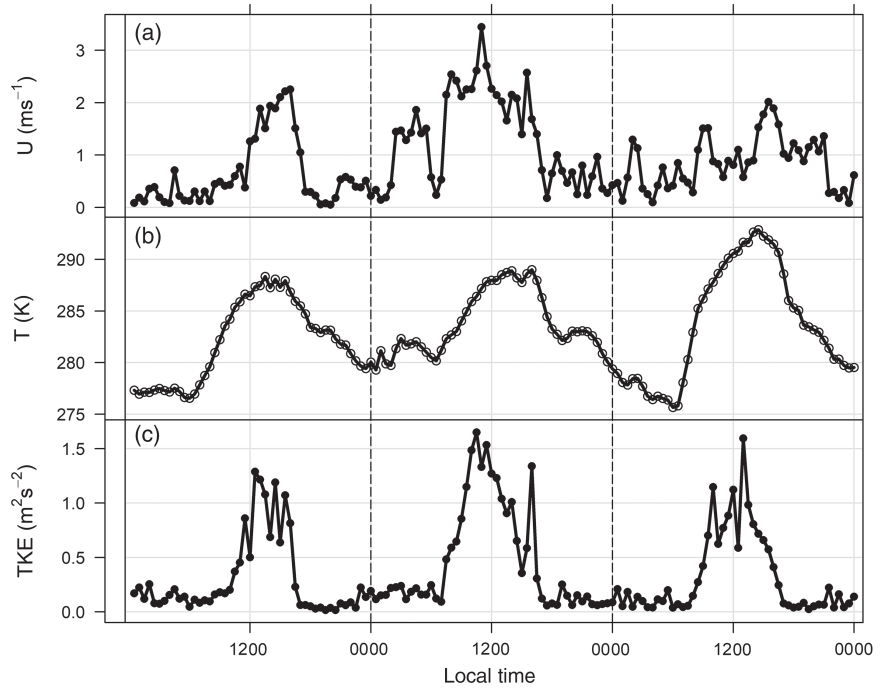

Figure 3. Meteorological parameters at a height of 3 m at the experimental site in Santa Maria, RS, Brazil between 29 April and 1 May 2016: (a) wind speed, U (m s^{-1}); (b) air temperature, T (K); and (c) turbulent kinetic energy (TKE) (m^2 s^{-2}).

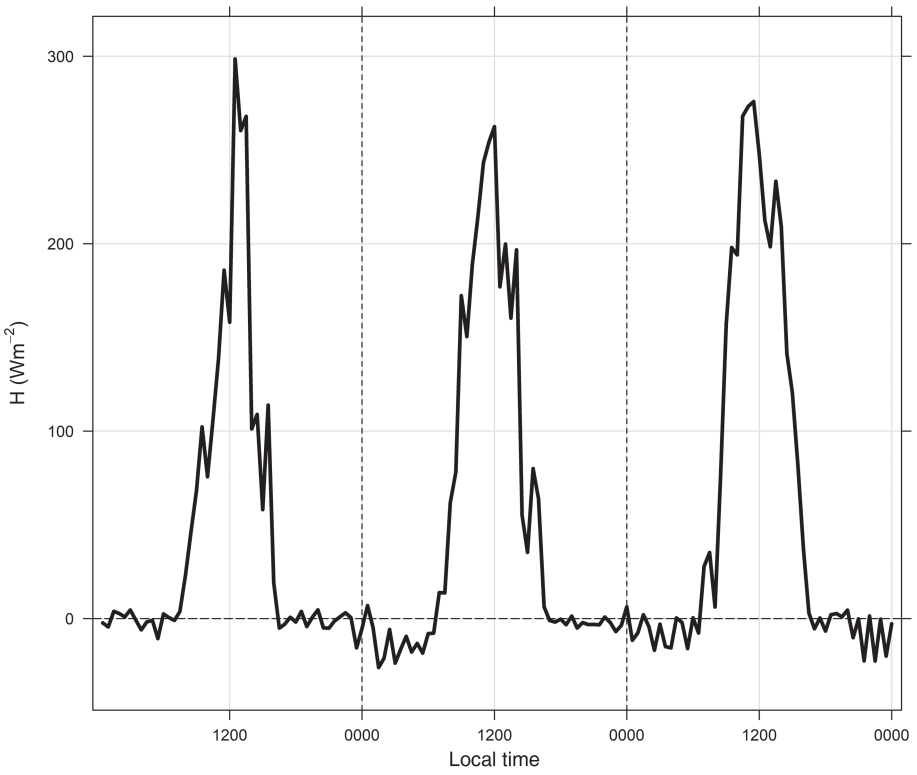

Figure 4. Turbulent heat flux, H (W m^{-2}), at the experimental site between 29 April and 1 May 2016.

greater than 1.0 m s^{-1} occurred (Figure 3(a)), and the downward turbulent sensible heat flux reached −10 w m^{-2} (Figure 4). This finding means that surface cooling is more efficiently transported to higher levels in the SBL, reducing the curvature of the potential temperature profile in the second half of the night (0300/0600 LT profiles of Figure 6). Therefore, the first regime from sunset to midnight lies within the classification of a radiative night, as proposed by André and Mahrt (1982), or as a 'very stable boundary layer' (Mahrt, 1998). From midnight to sunrise, however, a 'turbulent night' (André and Mahrt, 1982) or a 'weakly stable boundary layer' (Mahrt, 1998) occurs.

Table 3. Mean magnitudes of the Obukhov length (L) and Richardson numbers (Ri) for the night-time and daytime periods.

	29 April 2016 (0900–1700) LT	29–30 April 2016 (2000–0400) LT	30 April 2016 (0900–1700) LT	30 April–1 May 2016 (2000–0400) LT	1 May 2016 (0900–0700) LT	1 May 2016 (2000–0000) LT
L (m)	−9.90	5.26	−26.99	1.74	−24.08	1.41
Ri	−0.15	0.05	−0.11	0.14	−0.23	0.14

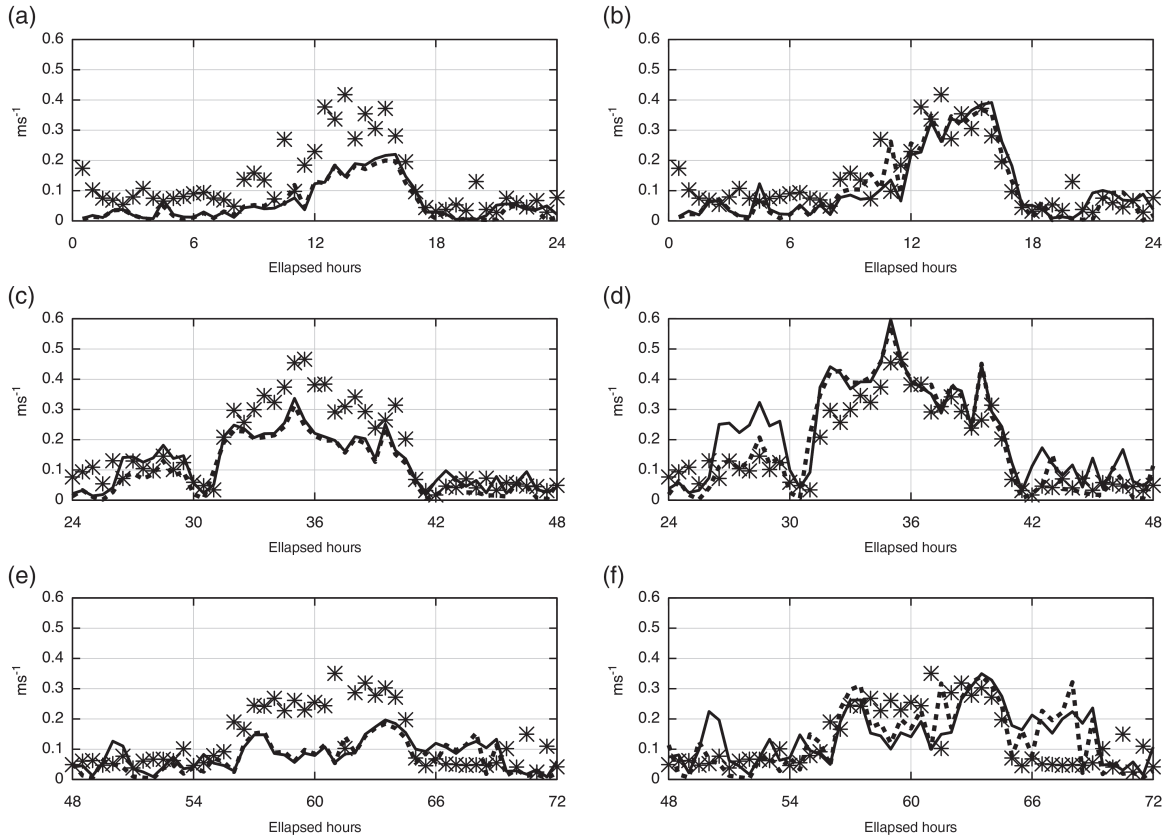

Figure 5. Comparison between the experimental friction velocity (asterisks) and the similarity expressions obtained using the B71 (continuous line) and BH91 (dashed line) stability correction functions for 29 April (a, b), 30 April (c, d) and 1 May 2016 (e, f). The left panels (a, c, e) are calculated using $z_0 = 0.05$ m, while the right panels (b, d, f) are calculated using $z_0 = 0.30$ m.

Table 4. Statistical analysis using R Package for the B71 and BH91 functions.

	B71	BH91
PBIAS	−22.2%	−9.90%
R	81.0%	81.00%

PBIAS, percentage bias; *R*, correlation co-efficient.

Table 5. Critical periods with extremely low wind speed conditions.

Period	From (LT)	To (LT)	Day
P1	0000	0600	29 April 2016
P2	1800	0600	29–30 April 2016
P3	1800	0600	30 April–1 May 2016

During the first period, the surface inversion heights are of the order of 300 m. Between this surface inversion and the free atmosphere lies the residual layer. This layer can be seen in Figure 6 as a quasi-neutrally stratified vertical region originating from the decay of turbulence of the previous diurnal CBL. As a consequence of the effect of the turbulence acting between 0300 LT and 0600 LT, the height of the NSI thickens.

3.3. Daytime temperature profiles

Figure 7 shows the vertical profile of the potential temperatures for 1 May at 0900, 1200 and 1500 LT. This daytime period was completely cloud free, and therefore the turbulent characteristics follow the patterns of a typical CBL with a potential temperature gradient near the surface and a well-defined inversion height.

At 0900 LT, a quasi-adiabatic thermal profile is observed to 200 m, suggesting that this is the thickness of the newly formed CBL. Above that height, a stable layer is observed between 200 and 500 m. At 1200 LT, the CBL has grown over the entirety of this fossil neutral layer, such that the first lowest inversion can be identified at a height of approximately 900 m. The same persists at 1500 LT. By employing these observational data and the means of the sensible heat flux for this period, it is possible to evaluate the convective velocity scale as:

$$w_* = \left(\frac{g}{\theta}\overline{w'\theta'}z_i\right)^{1/3} \quad (2)$$

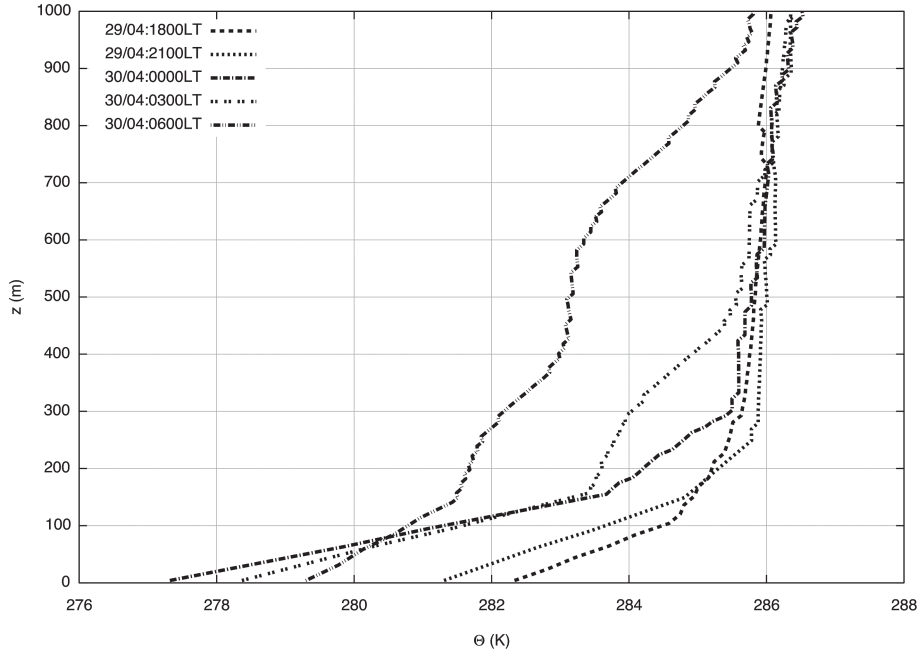

Figure 6. Potential temperature profiles in a stable boundary layer from 29 April at 1800 LT to 30 April 2016 at 0600 LT.

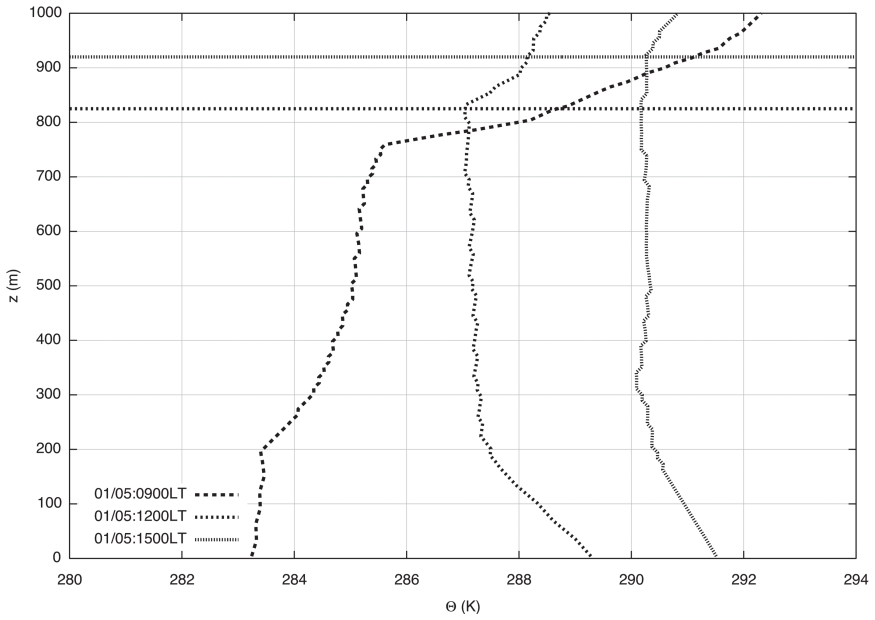

Figure 7. Potential vertical temperature profiles for 1 May 2016 at 0900, 1200 and 1500 LT, and estimation of the height of the planetary boundary layer (PBL) (horizontal lines).

where $\overline{w'\theta'}$ is the turbulent sensible heat flux; g is the acceleration due to gravity; and $\overline{\theta}$ is the mean potential temperature. Therefore, for the afternoon period in convective conditions, the magnitude of w_* was estimated to be of the order of 1.5 m s^{-1}. This magnitude agrees with the values suggested by Garratt (1992, p. 247). The characteristic time given by the ratio between z_i and w_* is in the order of 10 min and represents the time for a fluid particle undergoing the action of convective circulation to travel from the surface to the height of the first inversion. Additionally, Obukhov lengths in this convective period of the PBL assumed magnitudes between −10.8 and −42.5 m. The intensity of the convective effect in the unstable PBL can also be evaluated by the ratio z_i/L. The ratios range from −76.8 to −21.8, with friction velocity varying between 0.24 and 0.35 m s^{-1}. These micrometeorological parameters indicate that a large extension of the PBL is dominated by large convective eddies.

3.4. Turbulent spectra

The turbulent velocity energy spectrum directly demonstrates the distribution of energy with respect to frequency (Caughey and Palmer, 1979; Panofsky and Dutton, 1984). In particular, the identification of the frequencies associated with the spectral energy peaks merits closer examination. These peak frequencies f_m describe the spatial and temporal scales of the energy-containing eddies, which are responsible for the turbulent

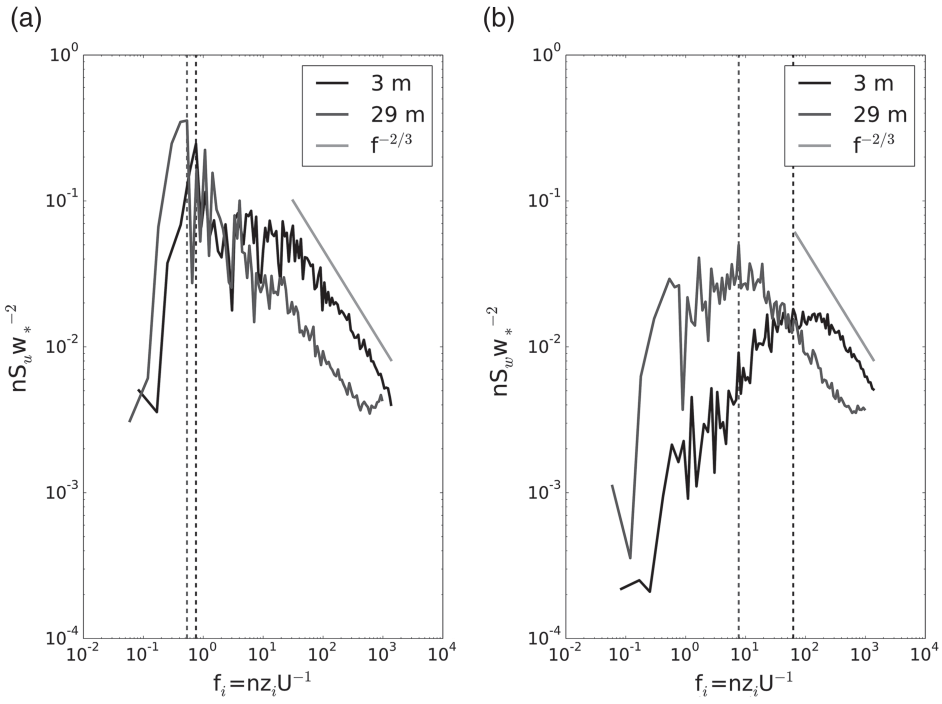

Figure 8. Turbulent convective energy spectra for the (a) *u* and (b) *w* wind components.

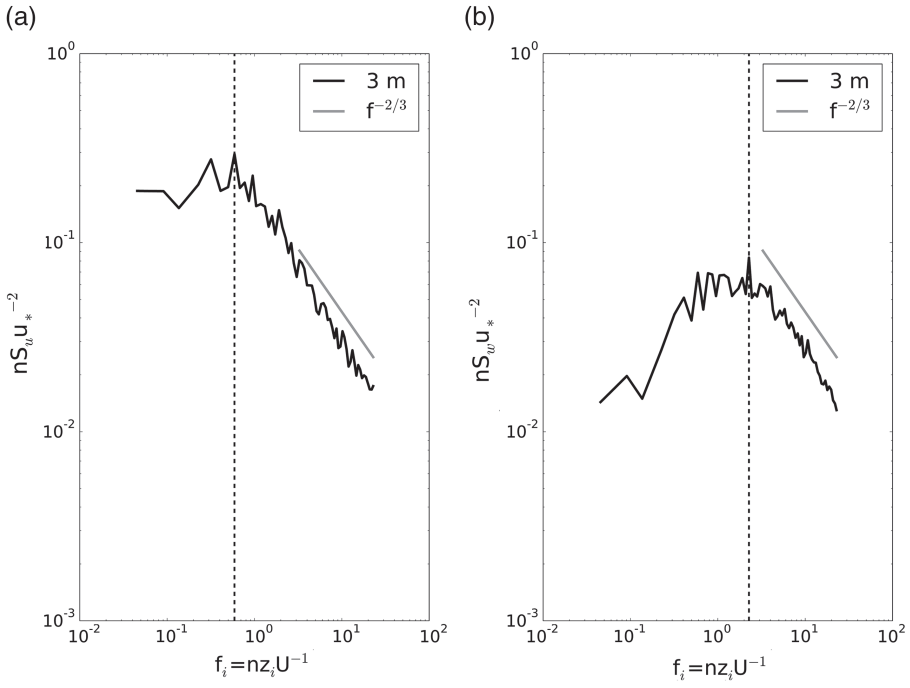

Figure 9. Turbulent stable energy spectra for the (a) *u* and (b) *w* wind components.

transport of scalar and vector species in the PBL. Figure 8 shows the turbulent convective energy spectrum for the *u* and *w* velocity components at heights of 3 and 29 m at 1200 LT. On the other hand, Figure 9 represents the averaged spectral curve at 3 m for the SBL at 2300 LT. Both stable and convective spectra were calculated for 1 May. Note that the stable spectra of the wind velocity components are dominated by low-frequency motions located in spectral regions that are normally not occupied by turbulent motion. Therefore, to filter out these large-scale movements, it is common to evaluate the spectra using shorter series (Vickers and Mahrt, 2006). In the present analysis, a 1 h time series is divided into twenty 3 min intervals.

Figures 8 and 9 show that the spectrum for the *u* horizontal component is larger at low frequencies than that for the *w* vertical component. The presence of the surface inhibits the manifestation of large eddies in the vertical plane. As a consequence of this surface impedance of the velocity components, in a convective case the *w* spectrum exhibits the largest variation with height (Panofsky and Dutton, 1984).

The peak values for the convective u spectrum associated with the non-dimensional peak frequencies ($f_m z_i/U$) for heights of 3 and 29 m are 0.76 and 0.53, respectively, yielding the following peak wavelengths of $(\lambda_m)_u$: 1.3 and 1.8 z_i. These results for the horizontal plane are in agreement with the 1.5 z_i obtained from measurements taken in a well-developed CBL (Caughey and Palmer, 1979). These results also indicate a tendency for the peak wavelengths of the horizontal velocity to be the same, independent of height. On the other hand, the peak frequencies for the convective w spectrum at heights of 3 and 29 m are 62.45 and 7.67, respectively, resulting in $(\lambda_m)_w = 0.016$ and 0.13 z_i. These magnitudes of $(\lambda_m)_w$ are of the same order as those observed in the Kansas data, and conform with free-convection behaviour (Kaimal *et al.*, 1972). The stable u and w spectra peak frequencies are 0.59 and 2.23, respectively, yielding$(\lambda_m)_u = 5.36$ m and$(\lambda_m)_w = 1.36$ m, respectively. Knowledge about these wavelengths can be used to provide dispersion parameters, such as eddy diffusivities and integral time scales, in Eulerian and Lagrangian diffusion models to evaluate the concentration fields originating from distinct contaminant sources.

4. Conclusions

The Pampa-2016 experimental campaign was performed in a typical Pampa lowland South American region. The campaign consisted of both surface flux measurements (at heights of 3 and 29 m) and radiosondes launched every 3 h. The resulting meteorological observations allowed for the analysis of turbulent properties associated with both stable and convective boundary layers.

The analysis of surface data has proven that under unstable conditions (daytime), the micrometeorological quantities, such as Obukhov length and friction velocity in the noon and afternoon periods, have the typical magnitudes of a well-developed convective boundary layer (CBL). Furthermore, the ratio z_i/L shows that convective turbulent structures dominate the major part of the atmospheric boundary layer (ABL). On the other hand, the analysis of night-time surface data shows that under stable conditions, for wind speeds close to zero, the prediction of friction velocity using the Monin–Obukhov theory (Garratt, 1992) provides unrealistic values that are very close to zero. This is an undesirable situation for numerical models which requires further investigation.

Furthermore, this experimental field campaign has provided meteorological profiles of temperature and wind. The combined analysis of the continuous surface measurements of the flux tower and temperature vertical soundings have shown that the nocturnal surface inversion (NSI), which occurs in calm wind situations, is basically generated by the radiative cooling mechanism that is set up after the late afternoon transition. The present analysis noted that the NSI height is close to 300 m at 1800 LT. Above this height, there is a deep residual layer, characterized by the near-adiabatic temperature profile. Therefore, in the first half of the night (between 1800 and 0000 LT), the height of the surface inversion has a smooth variation. At later times (after 0000 LT), when mean wind speed magnitudes increase, the temperature vertical profiles present positive curvatures in some specific levels of the stable boundary layer (SBL), demonstrating the fact that turbulent effects begin to cool the stable boundary layer (Figure 6).

The analysis of the convective temperature profiles was performed by considering radiosounding data launched on 1 May at 0900, 1200 and 1500 LT. This day presented a clear-sky environment which is favourable for the development of a typical CBL. The temperature profiles at 1200 and 1500 LT showed a near-surface unstable layer. Above this layer in the mixed layer, the strong convective turbulence homogenizes the temperature gradients which become negligible. The resulting adiabatic layer extends vertically to the base of the lowest inversion. This characteristic depth defines the height of the CBL and allows for the estimation of the convective velocity scale w_*. At noon and in the mid-afternoon, the CBL height is of the order of 900 m, resulting in a convective velocity scale of the order of 1.5 m s^{-1} and a convective time scale close to 10 min which is a typical value in a CBL (Sorbjan, 1997).

The observed spectra of the velocity components have provided important information regarding the spectral peak wavelengths. The magnitudes of the peak wavelength for the convective u component, measured at heights of 3 and 29 m, show a tendency for $(\lambda_m)_u$ to assume a value close to 1.5 z_i. This magnitude characterizes the horizontal dimension of long-lived convective structures that almost entirely fill the vertical space of the ABL. Conversely, the peak wavelengths for the convective w component noticeably increase with height, meaning that in the vertical plane in higher regions of the CBL, larger convective eddies find space to develop. Furthermore, the values for the convective $(\lambda_m)_w$ follow the free-convection prediction. The observed peak wavelength magnitudes for the stable u and w components sampled at height 3 m show that $(\lambda_m)_u$ assumes a value four times larger than $(\lambda_m)_w$. These peak wavelengths, estimated from the observed spectra, are generally used in equations that provide the turbulent parameters (eddy diffusivities and integral time scales) for distinct types of diffusion models.

The Pampa-2016 field campaign has provided useful information on the turbulent features of a lowland South American site for which there are relatively few observational studies concerning meteorological and micrometeorological aspects. Future studies can address important issues, such as air pollution modelling, wind energy and numerical simulation at both a turbulence-resolving scale (large-eddy simulation) and mesoscale circulation (numerical weather prediction).

Acknowledgements

The Pampa-2016 campaign was supported by the Ciências sem Fronteiras Conselho Nacional de Desenvolvimento Científico e Tecnológico (CNPq) program (contract number 401684/2013-0). The authors thank the Brasilian Coordenação de Aperfeiçoamento de Pessoal de Nível Superior (CAPES) for the partial financial support of this work. A special thanks to Ronald Buss de Sousa, Senior Scientist at the National Institute for Space Research (INPE) for his help in the field campaign.

References

Anabor V, Stensrud DJ, de Moraes OL. 2009. Simulation of a serial upstream-propagating mesoscale convective system event over southeastern South America using composite initial conditions. *Mon. Weather. Rev.* **137**: 2144–2163.

André J, Mahrt L. 1982. The nocturnal surface inversion and influence of clear-air radiative cooling. *J. Atmos. Sci.* **39**: 864–878.

Andreas EL, Mahrt L, Vickers D. 2015. An improved bulk air–sea surface flux algorithm, including spray-mediated transfer. *Q. J. Roy. Meteorol. Soc.* **141**: 642–654.

Beljaars A, Holtslag A. 1991. Flux parameterization over land surfaces for atmospheric models. *J. Appl. Meteorol.* **30**: 327–341.

Blay-Carreras E, Pino D, Vilà-Guerau de Arellano J, Van de Boer A, De Coster O, Darbieu C, *et al.* 2014. Role of the residual layer and large-scale subsidence on the development and evolution of the convective boundary layer. *Atmos. Chem. Phys.* **14**: 4515–4530.

Businger JA, Wyngaard JC, Izumi Y, Bradley EF. 1971. Flux-profile relationships in the atmospheric surface layer. *J. Atmos. Sci.* **28**: 181–189.

Carvalho JC, Degrazia GA, Anfossi D, Goulart AG, Cuchiara GC, Mortarini L. 2010. Simulating the characteristic patterns of the dispersion during sunset pbl. *Atmos. Res.* **98**: 274–284.

Caughey SJ. 1984. Observed characteristics of the atmospheric boundary layer. In *Atmospheric Turbulence and Air Pollution Modelling*. Springer: Dordrecht; 107–158.

Caughey S, Palmer S. 1979. Some aspects of turbulence structure through the depth of the convective boundary layer. *Q. J. Roy. Meteorol. Soc.* **105**: 811–827.

Garratt JR. 1992. *The Atmospheric Boundary Layer, Cambridge Atmospheric and Space Science Series*. Cambridge University Press: Cambridge, UK.

Goulart A, Degrazia G, Rizza U, Anfossi D. 2003. A theoretical model for the study of convective turbulence decay and comparison with large-eddy simulation data. *Bound.-Lay. Meteorol.* **107**: 143–155.

Grimm AM, Barros VR, Doyle ME. 2000. Climate variability in southern south america associated with el niño and la niña events. *J. Climate* **13**: 35–58.

Hoover JD, Stauffer DR, Richardson SJ, Mahrt L, Gaudet BJ, Suarez A. 2015. Submeso motions within the stable boundary layer and their relationships to local indicators and synoptic regime in moderately complex terrain. *J. Appl. Meteorol. Climatol.* **54**(2): 352–369.

Kaimal JC, Wyngaard J, Izumi Y, Coté O. 1972. Spectral characteristics of e surface-layer turbulence. *Q. J. Roy. Meteorol. Soc.* **98**: 563–589.

Licor L. 2015. *Eddypro 6.0 – Eddy Covariance Software*. LI-COR Inc, Lincolnm, ME.

Mahrt L. 1998. Nocturnal boundary-layer regimes. *Bound.-Lay. Meteorol.* **88**: 255–278.

Panofsky HA, Dutton JA. 1984. *AtmosphericTurbulence: Modelsand-Methods for EngineeringApplications*. John Wiley& Sons: New York, NY.

R Core Team. 2015, 2014. *R: A Language and Environment for Statistical Computing* [Internet]. R Foundation for Statistical Computing: Vienna.

Reuder J, Ablinger M, Agústsson H, Brisset P, Brynjólfsson S, Garhammer M, *et al.* 2012. FLOHOF 2007: an overview of the mesoscale meteorological field campaign at Hofsjökull, Central Iceland. *Meteorol. Atmos. Phys.* **116**: 1–13.

Rizza U, Miglietta MM, Acevedo OC, Anabor V, Degrazia GA, Goulart AG, *et al.* 2013b. Large-eddy simulation of the planetary boundary layer under baroclinic conditions during daytime and sunset turbulence. *Meteorol. Appl.* **20**: 56–71.

Rizza U, Miglietta M, Degrazia G, Acevedo O, Marques FE. 2013a. Sunset decay of the convective turbulence with large-eddy simulation under realistic conditions. *Physica A.* **392**: 4481–4490.

Sorbjan Z. 1997. Decay of convective turbulence revisited. *Bound.-Lay. Meteorol.* **82**(3): 503–517.

Trini Castelli S, Falabino S, Mortarini L, Ferrero E, Richiardone R, Anfossi D. 2014. Experimental investigation of surface-layer parameters in low wind-speed conditions in a suburban area. *Q. J. Roy. Meteorol. Soc.* **140**: 2023–2036.

Vickers D, Mahrt L. 2006. A solution for flux contamination by mesoscale motions with very weak turbulence. *Bound.-Lay. Meteorol.* **118**: 431–447.

